Proceedings of the
Annual Stability Conference
Structural Stability Research Council
Nashville, Tennessee, March 24-27, 2015

Automated buckling mode identification of thin-walled structures from 3D finite element mode shapes or point clouds

Junle Cai[1], Cristopher D. Moen[2]

Abstract
A Generalized Beam Theory (GBT) approach is derived that performs automated, quantitative modal decomposition of thin-walled members with an open cross-section. The technique extracts modal amplitudes and modal participation factors from any 3D displacement field, for example from finite element analysis or point clouds measured in the lab during a test to collapse. Thin-walled members exhibit deformation that can be represented as combinations of cross-sectional and global buckling modes. It is useful to quantitatively decompose these modes for strength prediction and design code development. Conventionally, buckling mode participation has been determined by visual inspection. This process is subjective and tedious since the person conducting the inspection is often dealing with many models or experiments. Taking advantage of GBT kinematics, the proposed method distinguishes itself by using only the GBT cross-section deformation modes instead of member-wise basis functions. The method is by nature applicable to different boundary and loading conditions without recalculation of basis functions. The mechanics are formulated to show that the method is supported by GBT kinematic assumptions, which ensures its general applicability. The approach is implemented in a Graphical User Interface (GUI) that accepts a thin-walled member 3D displacement field as input and then calculates modal participation factors, i.e., for member local, distortional, and global (Euler) buckling.

1 Introduction

The buckling phenomenon of open cross-section thin-walled structures is usually classified by three fundamental types: global (G) buckling; distortional (D) buckling; and local (L) buckling. These buckling mechanisms have different impacts on the post-buckling behavior: generally, global buckling has minimal post-buckling reserve, while cross-sectional modes like distortional buckling and local buckling have post-buckling capacity that can be utilized.

The Direct Strength Method, which is adopted in AISI-S100-12 (AISI-S100 2007) and the Australian/New Zealand Standard (Hancock 2007), predicts cold-formed steel member capacity with global (G), distortional (D), or local (L) buckling limit states using formulas with global or

[1]Ph.D. Candidate, Civil & Environmental Engineering, Virginia Tech, <junlecai@vt.edu>
[2]Associate Professor, Civil & Environmental Engineering, Virginia Tech, <cmoen@vt.edu>

cross-sectional slenderness as input. As long as codes and standards treat G, D, and L modes separately, proper buckling modal identification for both Finite Element (FE) Analysis and experiments is necessary. Modal identification can be exploited to quantitatively determine the nature of the buckling mode shape gained from FEA or test-based measurement, thus subjective and tedious visual inspection can be avoided. Modal identification is also helpful for research and code development, so that the failure mechanisms in FEA or experiments can be quantitatively categorized (Li et al. 2013; Salomon et al. 2015).

There are two existing methods that perform modal identification. The constrained finite strip method (cFSM) treats the modal amplitude calculation as a least squares problem which minimizes the error between member-wise displacement fields and reconstructed displacement fields (Ádány et al. 2010). The motivation is to approximate any FEA displacement fields by the linear combination of the cFSM basis functions. The cFSM basis functions, which depend on the member length and boundary conditions, are obtained in advance. Another method is based on the Generalized Beam Theory (GBT) stiffness matrix (Nedelcu 2012, 2014; Nedelcu and Cucu 2014). This method solves linear equation systems for modal amplitudes at discrete cross-sections along the member. In the linear equation system, the coefficient matrix is the GBT stiffness matrix and the right-hand side vector is calculated by substituting the displacement fields from Finite Element Analysis (FEA) into GBT formulas for evaluating stiffness terms. Then modal participation factors can be evaluated using modal amplitudes along the member.

This paper introduces a method utilizing GBT mode shapes as basis functions, and obtains modal amplitudes by solving a small-scale least squares problem at discrete cross-sections along a thin-walled member. The method utilizes concepts from both existing cFSM and GBT methods and has the following merits: (i) a single set of basis functions that can be used for any boundary conditions or member length; (ii) basis functions are easy to obtain as simply being GBT mode shapes; (iii) once GBT mode shapes and displacement fields are known, modal identification can be carried out without the knowledge of GBT assumptions about the displacement fields and constitutive law for calculating the stiffness terms, and without complex integrals for evaluating stiffness terms. Derivation and validation are provided in the following sections, demonstrating the method's general applicability.

2 Brief Review of Generalized Beam Theory

Generalized Beam Theory (Schardt 1989) is an extension of traditional beam theory as it describes the behavior of a beam by a system of fourth-order differential equations and takes into account cross-sectional distortion. As an ideal tool for analyzing thin-walled members, GBT is able to evaluate the participation of global, distortional, and local modes separately and explicitly (Silvestre et al. 2011). GBT employs Vlasov's null membrane assumption and Kirchhoff-Love plate theory, as follows (Camotim et al. 2010):

$$\begin{aligned}
&\varepsilon_{zz} = \gamma_{xz} = \gamma_{sz} = 0 && \varepsilon_{ss}^{M,L} = 0 && \gamma_{xs}^{M,L} = 0 \\
&\varepsilon_{xx}^{M,L} = u_{,x} && \varepsilon_{xx}^{M,NL} = (v_{,x}{}^2 + w_{,x}{}^2)/2 && \gamma_{xs}^{M,NL} = w_{,s} w_{,x} \\
&\varepsilon_{xx}^{B} = -z w_{,xx} && \varepsilon_{s}^{B} = -z w_{,ss} && \gamma_{xs}^{B} = -2 z w_{,sx}
\end{aligned} \tag{1}$$

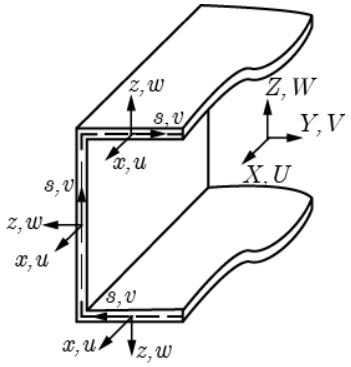

Figure 1: Coordinate system and translations for a thin-walled member

where (i) $(\cdot)_{,x}=\partial(\cdot)/\partial x$, (ii) superscripts $(\cdot)^M$, $(\cdot)^B$ denote membrane strain and bending strain, respectively, (iii) superscripts $(\cdot)^L$, $(\cdot)^{NL}$ stand for linear and nonlinear terms, and (iv) $\varepsilon_{ss}^{M,L}=0$, $\gamma_{xs}^{M,L}=0$ represents Vlasov's null membrane strain assumption.

In the context of GBT, the displacement field of the cross section mid-line is related to GBT mode shapes and modal amplitudes (or modal amplitude derivatives), as follows:

$$u(s,x)=\sum_{k=1}^{n}u_k(s)\phi_k'(x) \qquad v(s,x)=\sum_{k=1}^{n}v_k(s)\phi_k(x) \qquad w(s,x)=\sum_{k=1}^{n}w_k(s)\phi_k(x) \tag{2}$$

where (i) $u_k(s)$, $v_k(s)$, and $w_k(s)$ are functions specifying GBT cross-sectional mode shapes, (ii) $\phi_k(x)$ is the modal amplitude vector at location x, and (iii) s is the line coordinate around the cross-section. Warping deformation $u_k(s,x)$ is related to the first-order derivatives of modal amplitudes.

Stress components are related to strains by the constitutive law in Eq. (3):

$$\sigma_{xx}^{M}=E\varepsilon_{xx}^{M}, \quad \begin{Bmatrix}\sigma_{xx}^{B}\\ \sigma_{ss}^{B}\\ \tau_{xs}^{B}\end{Bmatrix}=\begin{bmatrix}\frac{E}{1-\nu^2} & \frac{\nu E}{1-\nu^2} & 0\\ \frac{\nu E}{1-\nu^2} & \frac{E}{1-\nu^2} & 0\\ 0 & 0 & G\end{bmatrix}\begin{Bmatrix}\varepsilon_{xx}^{B}\\ \varepsilon_{ss}^{B}\\ \gamma_{xs}^{B}\end{Bmatrix} \tag{3}$$

where (i) E,ν,G are elastic modulus, Poisson's ratio, and shear modulus, respectively, and (ii) σ_{ij}, ε_{ij} are stress and strain components.

To acquire a differential equation of equilibrium, the Principle of Virtual Work is utilized, i.e.,

$$\delta V=\delta U+\delta \Pi \tag{4}$$

where δV is the variation of total potential energy, δU is the variation of strain energy, and $\delta \Pi$ is the variation of potential energy with respect to the pre-buckling reference stress.

By expressing strain variation in terms of modal amplitude variation $\delta\phi_i$ and accounting for the virtual work performed by every stress component, the GBT differential-equation system for an eigen-buckling problem is obtained ((Davies et al. 1994) :

$$C_{ik}\phi_{k,xxxx} - D_{ik}\phi_{k,xx} + B_{ik}\phi_k - \lambda X_{jik}(W_j^0\phi_{k,x})_{,x} = 0\,. \tag{5}$$

This ordinary differential equation system (i being a free index) represents equilibrium for each GBT mode. In Eq. (5), W_j^0 is the pre-applied force resultant corresponding to axial load (j=1), major axis bending moment (j=2), minor axis bending moment (j=3), and torsional warping bimoment (j=4). Other terms are:

$$\begin{aligned}
C_{ik} &= C_{ik}^1 + C_{ik}^2 = \frac{Et}{1-\nu^2}\int_b u_i u_k ds + \frac{Et^3}{12(1-\nu^2)}\int_b w_i w_k ds,\\
B_{ik} &= \frac{t^3}{12(1-\nu^2)}\int_b w_{i,ss} w_{k,ss} ds,\\
D_{ik} &= D_{ik}^1 - (D_{ik}^2 + D_{ki}^2) = \frac{Gt^3}{3}\int_b w_{i,s} w_{k,s} ds - \frac{\nu Et^3}{12(1-\nu^2)}\int_b (w_i w_{k,ss} + w_k w_{i,ss}) ds,\\
X_{jik} &= \int_b \frac{u_j t}{C_{jj}}(v_i v_k + w_i w_k) ds
\end{aligned} \tag{6}$$

where C_{ik} represents the stiffness with regard to warping, D_{ik} represents the stiffness with regard to torsion, and B_{ik} represents the in-plane bending stiffness when the cross-section does not remain rigid, which only exists for modes 5 and above. The tensor X_{jik} represents the geometric stiffness with regard to the pre-applied force resultant W_j^0.

The GBT cross-sectional mode shapes $u_k(s)$, $v_k(s)$, and $w_k(s)$ are determined by 'cross-sectional analysis' (Gonçalves et al. 2010), which solves for mode shapes by simultaneously diagonalizing matrices C and B in Eq. (5). Fig. 2 shows a lipped channel with dimensions, material properties, and the GBT cross-sectional discretization. Fig. 3 shows the first 18 GBT mode shapes for the cross section. There are two sets of nodes in GBT cross-sectional analysis, namely natural nodes and intermediate nodes. Natural nodes are intersections of fold lines, and intermediate nodes are discretization nodes between natural nodes. End nodes are both natural nodes and intermediate nodes.

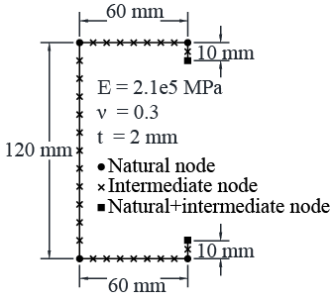

Figure 2: Channel cross section - material properties, dimensions, GBT discretization

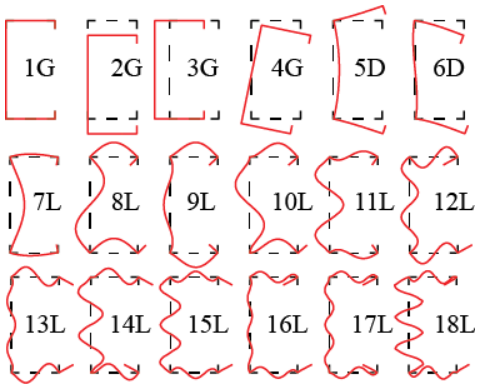

Figure 3: GBT mode shapes - G for global buckling, D for distortional buckling, and L for local buckling

3 Buckling Mode Identification Method

In a general buckling problem, several buckling modes are mixed and they interact with each other (Dinis and Camotim 2011). In the context of GBT, the interaction is taken into account by coupled stiffness terms, e.g., matrix D and X in Eq. (5) above are coupled as off-diagonal terms are present. However in-plane displacement fields are linear combinations of buckling mode shapes without coupling, where the weighting function is the modal amplitude vector, as shown in Eq. (2).

Therefore, in this paper, the modal amplitude vector $\phi_k(x)$ in Eq.(2) is solved by substituting $u_k(s)$, $v_k(s)$, and $w_k(s)$ obtained by 'cross-sectional analysis' and $u(s,x)$, $v(s,x)$, $w(s,x)$ obtained from a general 3d displacement field, for example, a specific mode from a thin shell finite element eigen-buckling analysis or from measured point cloud data during a column or beam test. Once the modal amplitude vector $\phi_k(x)$ is obtained at multiple discrete cross-sections along the member, member-wise modal participation can be evaluated as described in the next section.

3.1 Calculation of Modal Amplitudes at Given Cross-Section

If an open cross-section is discretized by n nodes, there are n+2 GBT modes. Beyond mode 1 for uniform compression, amplitudes of n+1 modes are to be quantified. These amplitudes, i.e., $\phi_k(x)$, can be found by solving the least squares problem in Eq.(7):

$$\sum_{k=2}^{n}\begin{bmatrix} V_k \\ W_k \end{bmatrix}_{2n\times(n+1)} \left\{ \phi_k(x) \right\}_{(n+1)\times 1} \overset{least\ square}{=} \left\{ \begin{matrix} V \\ W \end{matrix} \right\}_{2n\times 1} \tag{7}$$

in which (i) V_k, W_k are displacement components at discretization nodes of GBT mode k in the global coordinate system; once the GBT mode shapes $u_k(s)$, $v_k(s)$, and $w_k(s)$ as shown in Fig. 3 are obtained from the GBT cross-section analysis (Schardt 1989; Gonçalves et al. 2010) or by free software which conduct cross-sectional analysis (Bebiano R. et al. 2014; Cai 2014) , V_k, W_k can be readily obtained by coordinate transformation; (ii) $\phi_k(x)$ is the modal amplitude vector of mode k at location x along the member, (iii) V, W are in-plane displacements in the global coordinate system (as shown in Fig. 1) obtained by FEA or by test measurements, (iv) the

subscript denotes the dimensions of the matrix with *n* being the number of discretization nodes. The above equation is a linear optimization problem with *n+1* input arguments and *2n* objectives. For a general mathematical problem without physical meaning, the solution is challenging and possibly undefined because there are far more equations to solve than input arguments. However, because of Generalized Beam Theory kinematics, many of these *2n* equations are 'related', and the least squares problem can be solved with minimal error.

The justification for Eq. (7) is provided next. It is shown that: (i) only kinematics are used in the method once the mode shapes are known, i.e., no stiffness matrix is involved; (ii) the method is applicable to different loading and boundary conditions; and (iii) the error of the mode identification comes from the incompleteness of the GBT displacement field. Specifically, GBT utilizes Vlasov's null membrane strain assumption, which forces the local displacement *v* to be a constant in each fold line, and transverse extension is not captured.

The justification of Eq. (7) is demonstrated through an illustrative example shown in Fig. 4 by four steps. The cross-section has 8 nodes and 10 GBT modes with 9 modal amplitudes to be identified.

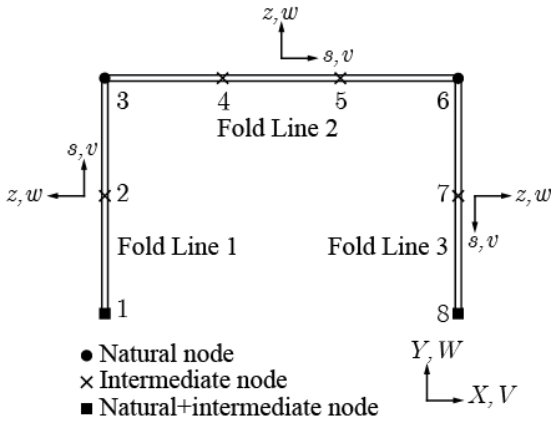

Figure 4: Illustrative cross section

3.1.1 Step 1 - Assuming Vlasov's assumption applies for the displacement field, and using v of fold lines and w of intermediate nodes to solve for $\{\phi_k\}$.

Since Vlasov's assumption applies at this stage, the displacement *v* is a constant in each fold line (*FL*). Once *v* of all fold lines and *w* of intermediate nodes are obtained, a linear system to solve for $\{\phi_k\}$ can be written down as:

$$\begin{bmatrix} v_2^{FL.1} & v_3^{FL.1} & \dots & v_{10}^{FL.1} \\ v_2^{FL.2} & v_3^{FL.2} & \dots & v_{10}^{FL.2} \\ v_2^{FL.3} & v_3^{FL.3} & \dots & v_{10}^{FL.3} \end{bmatrix} \begin{Bmatrix} \phi_2 \\ \phi_3 \\ \dots \\ \phi_{10} \end{Bmatrix} = \begin{Bmatrix} v^{FL.1} \\ v^{FL.2} \\ v^{FL.3} \end{Bmatrix}, \tag{8a}$$

$$\begin{bmatrix} w_2^1 & w_3^1 & \dots & w_{10}^1 \\ w_2^2 & w_3^2 & \dots & w_{10}^2 \\ w_2^4 & w_3^4 & \dots & w_{10}^4 \\ w_2^5 & w_3^5 & \dots & w_{10}^5 \\ w_2^7 & w_3^7 & \dots & w_{10}^7 \\ w_2^8 & w_3^8 & \dots & w_{10}^8 \end{bmatrix} \begin{Bmatrix} \phi_2 \\ \phi_3 \\ \dots \\ \phi_{10} \end{Bmatrix} = \begin{Bmatrix} w^1 \\ w^2 \\ w^4 \\ w^5 \\ w^7 \\ w^8 \end{Bmatrix}. \tag{8b}$$

where: (i) superscript $(\cdot)^{FL.i}$ stands for the i^{th} fold line; (ii) $(\cdot)^j$ stands for the j^{th} node, noting that nodes (1,2,4,5,7,8) are intermediate nodes; and (iii) subscript $(\cdot)_k$ stands for the k^{th} GBT mode. Eq. (8) can be written compactly as:

$$\sum_{k=2}^{n} \begin{bmatrix} v_k^{Fold\ Line} \\ w_k^{Inter.\,Node} \end{bmatrix} \{\phi_k\} = \begin{bmatrix} v^{Fold\ Line} \\ w^{Inter.\,Node} \end{bmatrix}. \tag{9}$$

Eq. (9) is a linear system with 9 equations to solve for 9 unknowns (ϕ_2~ϕ_{10}). Since the mode shapes are linearly independent as displacement-field basis functions, the solution is readily obtained by solving a determined linear system.

3.1.2 Step 2 - Still assuming Vlasov's assumption applies, but using v and w of all nodes (intermediate and natural) to solve for $\{\phi_k\}$.

Eq. (9) in Step 1 can generate the modal amplitude vector $\{\phi_k\}$ if Vlasov's assumption applies. In Step 2, another linear system is shown to yield $\{\phi_k\}$ as well by illustrating the equivalence between Step 2 and Step 1. The linear system in Step 2 corresponds to displacements *v* and *w* of all nodes in local coordinate system (see Fig. 4 for convention of local coordinate system) as follows: :

$$\begin{bmatrix} v_2^1 & v_3^1 & \dots & v_{10}^1 \\ v_2^2 & v_3^2 & \dots & v_{10}^2 \\ \vdots & \vdots & \vdots & \vdots \\ v_2^8 & v_3^8 & \dots & v_{10}^8 \end{bmatrix} \begin{Bmatrix} \phi_2 \\ \phi_3 \\ \vdots \\ \phi_{10} \end{Bmatrix} = \begin{Bmatrix} v^1 \\ v^2 \\ \vdots \\ v^8 \end{Bmatrix}, \tag{10a}$$

$$\begin{bmatrix} w_2^1 & w_3^1 & \dots & w_{10}^1 \\ w_2^2 & w_3^2 & \dots & w_{10}^2 \\ \vdots & \vdots & \vdots & \vdots \\ w_2^8 & w_3^8 & \dots & w_{10}^8 \end{bmatrix} \begin{Bmatrix} \phi_2 \\ \phi_3 \\ \vdots \\ \phi_{10} \end{Bmatrix} = \begin{Bmatrix} w^1 \\ w^2 \\ \vdots \\ w^8 \end{Bmatrix}. \tag{10b}$$

Compactly:

$$\sum_{k=2}^{n} \begin{bmatrix} v_k \\ w_k \end{bmatrix} \{\phi_k\} = \begin{Bmatrix} v \\ w \end{Bmatrix}. \tag{11}$$

For interpretation, Eq. (10) is annotated in Fig. 5. In Eq. (10.a), since local displacement v is constant in each fold line, rows 1 to 3 in the red box all correspond to v in the first fold line, because nodes 1 to 3 belong to the first fold line (Natural nodes belong to two fold lines. For the justification, the local coordinate system of the natural node is taken with the fold line before it, e.g., node 3 uses the local coordinate system of fold line 1). The same consideration applies for the second and third fold lines, and thus Eq. (10a) is equivalent with Eq. (8a) in Step 1, as both of them involve v of all fold lines.

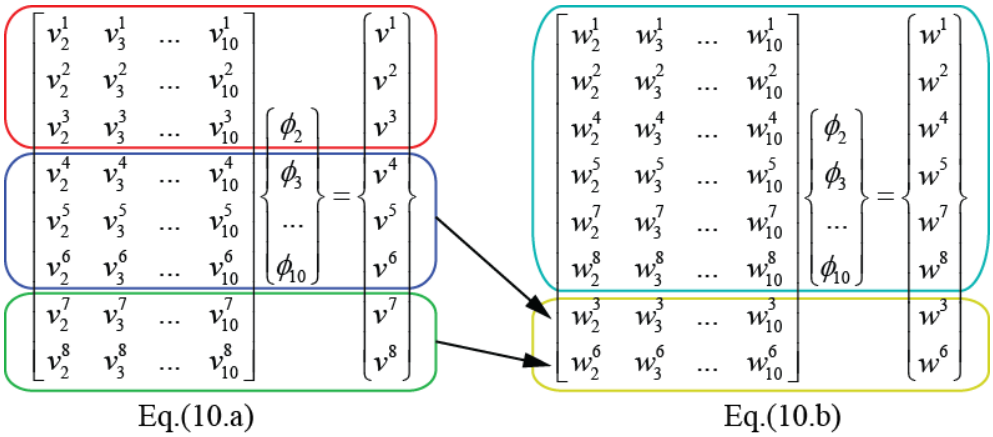

Figure 5: Equation (10) rewritten with annotations

For Eq. (10.b), the order of nodes 1 to 10 is rearranged in Fig. 5. The first part with intermediate nodes (1,2,4,5,7,8) in the cyan box is identical to Eq. (8.b) . The second part, in the yellow box, involves w^3 and w^6. Because node 3 and node 6 are at intersections of fold lines, w translations of intersections are equivalent to v displacements of adjacent fold lines.

Taking node 3 for example (see Fig. 6), w^3 is the horizontal displacement at node 3. This translation is related to local shifting in the second fold line as $w^3 = -v^{FL.2}$, in which $v^{FL.2}$ is already taken into account in Eqs. (8.a) and (10.a). The same type of derivation applies for node 6 as well.

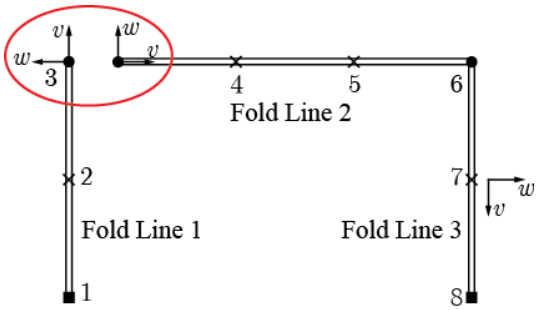

Figure 6: w^3 equals local shifting v in fold line 2 with a opposite sign

For a general case where fold lines do not meet at 90 degrees, it can still be shown that w of natural nodes (or intersections of fold lines) can be derived from v of adjacent fold lines from the kinematics in Fig. 7 and Eq. (12). Since v of fold lines are already taken into account in Eq. (8a) and (10a), these equations with intersections are linearly dependent on those equations (w^3 and w^6 in our example):

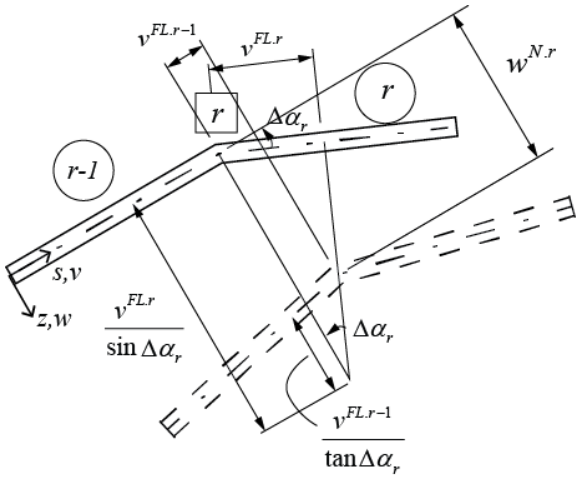

Figure 7: Dependence of *w* at natural node upon *v* of adjacent fold lines (Schardt 1989)

$$w^r = \frac{v^{FL.r}}{\sin\Delta\alpha_r} - \frac{v^{FL.r-1}}{\tan\Delta\alpha_r}. \tag{12}$$

Overall, the linear system in Step 2 is equivalent to the linear system in Step 1, as shown in Eq. (13). The kinematical relations are: (i) Vlasov's assumption makes *v* a constant in each fold line; (ii) *w* of any natural node (intersection of fold lines) is dependent upon *v* of adjacent fold lines. Hence, 9 linearly independent equations exist to solve for 9 unknowns (ϕ_2~ϕ_{10}), and the Step 2 system is linearly determined.

$$\sum_{k=2}^{n}\begin{bmatrix} v_k^{Fold\ Line} \\ w_k^{Inter.\ Node} \end{bmatrix}\{\phi_k\} = \begin{bmatrix} v^{Fold\ Line} \\ w^{Inter.\ Node} \end{bmatrix} \Leftrightarrow \sum_{k=2}^{n}\begin{bmatrix} v_k \\ w_k \end{bmatrix}\{\phi_k\} = \begin{Bmatrix} v \\ w \end{Bmatrix}. \tag{13}$$

3.1.3 Step 3 - Expressing linear system in Step 2 in the global coordinate system
In Step 3, all the coordinates of Step 2 are written in the global coordinate system:

$$\begin{bmatrix} V_2^1 & V_3^1 & \dots & V_{10}^1 \\ V_2^2 & V_3^2 & \dots & V_{10}^2 \\ \vdots & \vdots & \vdots & \vdots \\ V_2^8 & V_3^8 & \dots & V_{10}^8 \end{bmatrix}\begin{Bmatrix} \phi_2 \\ \phi_3 \\ \vdots \\ \phi_{10} \end{Bmatrix} = \begin{Bmatrix} V^1 \\ V^2 \\ \vdots \\ V^8 \end{Bmatrix}, \tag{14a}$$

$$\begin{bmatrix} W_2^1 & W_3^1 & \dots & W_{10}^1 \\ W_2^2 & W_3^2 & \dots & W_{10}^2 \\ \vdots & \vdots & \vdots & \vdots \\ W_2^8 & W_3^8 & \dots & W_{10}^8 \end{bmatrix}\begin{Bmatrix} \phi_2 \\ \phi_3 \\ \vdots \\ \phi_{10} \end{Bmatrix} = \begin{Bmatrix} W^1 \\ W^2 \\ \vdots \\ W^8 \end{Bmatrix}. \tag{14b}$$

Compactly:

$$\sum_{k=2}^{n}\begin{bmatrix} V_k \\ W_k \end{bmatrix}\{\phi_k\} = \begin{Bmatrix} V \\ W \end{Bmatrix}. \tag{15}$$

The concept of coordinate transformation is used to prove the equivalence between Stage 3 and Stage 2. Equations for an arbitrary node *r* in Stage 2 and Stage 3 are respectively:

$$\begin{bmatrix} v_k^r \\ w_k^r \end{bmatrix}\{\phi_k\} = \begin{Bmatrix} v^r \\ w^r \end{Bmatrix}. \tag{16}$$

$$\begin{bmatrix} V_k^r \\ W_k^r \end{bmatrix}\{\phi_k\} = \begin{Bmatrix} V^r \\ W^r \end{Bmatrix}. \tag{17}$$

Multiplying both sides of Eq. (17) by the coordinate transformation matrix between global and local coordinate systems (see Fig. 8), Eq. (18) is acquired:

$$\begin{bmatrix} \cos\alpha & \sin\alpha \\ -\sin\alpha & \cos\alpha \end{bmatrix}\begin{bmatrix} V_k^r \\ W_k^r \end{bmatrix}\{\phi_k\} = \begin{bmatrix} \cos\alpha & \sin\alpha \\ -\sin\alpha & \cos\alpha \end{bmatrix}\begin{Bmatrix} V^r \\ W^r \end{Bmatrix}. \tag{18}$$

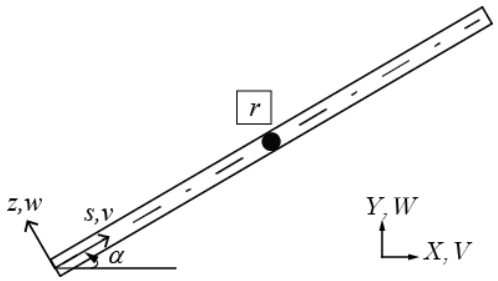

Figure 8: Coordinate transformation between global and local coordinate system

Because the coordinate transformation matrix is always invertible (the determinant of it is $\cos^2\alpha + \sin^2\alpha = 1$), Eq. (16) can be derived from Eq. (18). Applying the same derivation to all nodes, it is shown that Step 3 is equivalent to Step 2, as shown in Eq. (19):

$$\sum_{k=2}^{n}\begin{bmatrix} v_k \\ w_k \end{bmatrix}\{\phi_k\} = \begin{Bmatrix} v \\ w \end{Bmatrix} \Leftrightarrow \sum_{k=2}^{n}\begin{bmatrix} V_k \\ W_k \end{bmatrix}\{\phi_k\} = \begin{Bmatrix} V \\ W \end{Bmatrix}. \tag{19}$$

3.1.4 Step 4 - Realizing that Vlasov's assumption is not strictly applicable to FEA/experimental results, and transferring the linear system in Step 3 to a least squares problem

Generalized Beam Theory adopts Vlasov's assumption, which puts constraints on the local translation *v* in each fold line. However, in finite element analysis or test-measured point clouds, this constraint does not exist. Specifically, due to the presence of transverse membrane strain, local displacement *v* is not strictly constant (for better interpretation, Fig. 13 can be observed, as it shows a numerical example).

Because the transverse extension strain is always present in FEA or test-based measurement for a general case, no matter whether the 'GBT stiffness matrix method' or the method of this paper is used, the displacement fields cannot be perfectly reconstructed by GBT modes (in the context of conventional GBT modes without 'transverse extension' modes), and the Step 3 equation is now overdetermined. However, since the influence of transverse extension is minimal, GBT modal amplitudes can be found by reformulating Eq. (15) as a linear least squares problem

$$\min\left(\left|\sum_{k=2}^{n}\begin{bmatrix}V_k\\W_k\end{bmatrix}\{\phi_k\}-\begin{Bmatrix}V\\W\end{Bmatrix}\right|\right) \text{ or } \sum_{k=2}^{n}\begin{bmatrix}V_k\\W_k\end{bmatrix}\{\phi_k\} \overset{\text{least square}}{=} \begin{Bmatrix}V\\W\end{Bmatrix}. \tag{20}$$

This operation projects the in-plane displacement fields (V and W obtained from FEA for example) onto the sub-space of GBT solutions , as shown in Fig. 9.

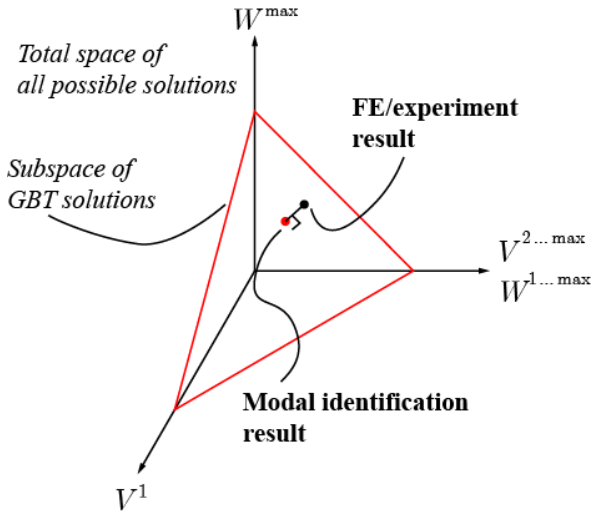

Figure 9 : Displacement field projection for calculating $\{\phi_k\}$

3.1.5 Summary: four-step justification of modal amplitudes calculation method

The four-step justification modal amplitude calculation method is summarized in Eq. (21). The equivalence of Step 1 and 2 results because of GBT kinematics, and for Steps 2 and 3 by coordinate transformation. Any equation in the first three steps will generate the exact solution of the modal amplitudes vector if the in-plane displacement field falls in the subspace of GBT solutions. The linear system in Step 3 is transferred to a least squares problem in Step 4 because of the presence of transverse extension. One reason for providing this four-step example is to show that the scheme is made possible by the rationality of GBT kinematics; otherwise the Step 4 equation generally does not give a satisfactory solution as a purely mathematical problem, because the number of objectives (*2n, e.g., 16 in the example above*) to be optimized is more than the number of input arguments (*n+1, e.g., 9 in the example above*).

$$\left(\sum_{k=2}^{n}\begin{bmatrix} v_k^{Fold\ Line} \\ w_k^{Inter.\ Node}\end{bmatrix}\{\phi_k\}=\begin{bmatrix} v^{Fold\ Line} \\ w^{Inter.\ Node}\end{bmatrix}\right)\Leftrightarrow\left(\sum_{k=2}^{n}\begin{bmatrix} v_k \\ w_k\end{bmatrix}\{\phi_k\}=\begin{Bmatrix} v \\ w\end{Bmatrix}\right)\Leftrightarrow\left(\sum_{k=2}^{n}\begin{bmatrix} V_k \\ W_k\end{bmatrix}\{\phi_k\}=\begin{Bmatrix} V \\ W\end{Bmatrix}\right)$$
$$\Rightarrow\left(\sum_{k=2}^{n}\begin{bmatrix} V_k \\ W_k\end{bmatrix}\{\phi_k\}\overset{least\ square}{=}\begin{Bmatrix} V \\ W\end{Bmatrix}\right). \tag{21}$$

3.2 Modal participation factors and error evaluation

Formulae to calculated modal participation factors using modal amplitudes have been proposed (Silvestre and Camotim 2002):

$$P_i=\int_L|\phi_i(x)|\,dx\,/\sum_{k=1}^{n}\int_L|\phi_k(x)|\,dx\,. \tag{22}$$

Once the modal amplitudes of discrete cross-sections along the member are obtained as described in the previous Section 3.1, Eq. (7), modal participation can be determined by the discrete form of Eq. (22), as shown in Eq. (23):

$$P_i=\sum_{\text{section}=1}^{N}|\phi_i(x_{\text{section}})|\,/\sum_{k=1}^{n}\sum_{\text{section}=1}^{N}|\phi_k(x_{\text{section}})|\,. \tag{23}$$

In addition with member-wise participation factor P_i, the modal participation factors at a given cross-section is evaluated as follows:

$$p_i(x)=|\phi_i(x)|\,/\sum_{k=1}^{n}|\phi_k(x)|\,. \tag{24}$$

With the notation, the member-wise participation factors P_i can be written as:

$$P_i=\int_L p_i(x)dx\,. \tag{25}$$

The error of the reconstructed displacement field from conducting modal identification can be evaluated using Eq. (26):

$$error=\sqrt{d_{err\text{-}VW}{}^{T}d_{err-VW}}\,\Big/\sqrt{d_{VW}{}^{T}d_{VW}}\,. \tag{26}$$

The displacement component U is absent in the expression since the warping is related to the derivatives of modal amplitudes ϕ_k' but not the amplitudes ϕ_k, and ϕ_k are what is needed for calculating modal participation factors.

4 Illustrative examples

Example 1 – thin-walled lipped Cee-section column

For the first illustrative example, modal identification is carried out on the result of an FEA eigen-buckling analysis of a column. The column cross section is the Cee shown in Fig. 2, with

the thickness of the channel being t = 2mm and the member length being L = 1240mm. The cross section is discretized into 32 sub-segments (2 equally wide pieces in each flange lip, 8 equally wide pieces in each flange, and 12 equally wide pieces in the web) for GBT cross-sectional analysis. A total of 35 GBT mode shapes are produced, and the first 18 GBT mode shapes are shown in Fig. 3.

To obtain the displacement field for performing modal identification, a shell finite element analysis (SFEA) is conducted using the commercial finite element program ABAQUS (Simulia 2012). The first 50 eigen-buckling solutions are recorded for further analysis. The member is meshed into 3936 rectangular elements. In the cross-sectional plane, the discretization is identical with GBT (shown in Fig. 2). In the longitudinal direction, the discretization is made every 10 mm, which results in 124 cross sections. The ABAQUS S4 element with finite membrane strain is used. In-plane translations (U_x, U_z) of nodes on both ends are fixed, and the longitudinal warping (U_y) is prescribed at all nodes on the mid-length cross section. Shell edge tractions q = 3.846N/mm are applied to both ends of the member, which corresponds to 1000N of compression force. FEA modal is shown in Fig. 10 and buckling modes in Fig. 11.

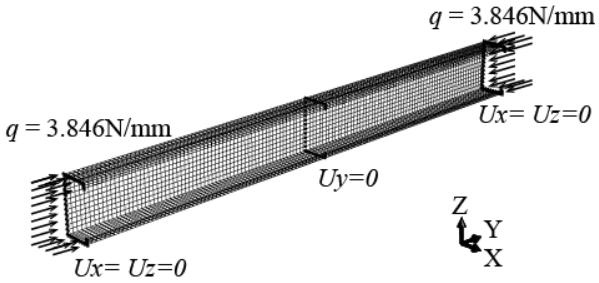

Figure 10: Example 1 - FEA modal boundary conditions

A custom-built MATLAB (MALAB 2010) GUI 'Buckling Cracker' (Cai 2014) with step-by-step video tutorial (Cai 2014) is programmed to perform the modal identification, and the displacement fields generated by SFEA are treated as input for the 'Buckling Cracker'. Modal participation and errors are evaluated by the code and shown in Table 1. Also, buckling mode shapes and corresponding modal amplitudes of the first 5 buckling modes are shown in Fig. 11.

Table 1:Example 1 - Modal participation and error for the first 10 buckling modes

Buckling mode	2G	3G	4G	5D	6D	7L	8-35L	error (%)
1	0.00	0.13	0.00	91.81	0.00	7.5	0.6	0.058
2	0.00	0.13	0.00	69.38	0.00	28.6	1.9	0.077
3	0.00	0.13	0.00	98.30	0.00	1.3	0.3	0.048
4	0.00	0.11	0.00	71.76	0.00	26.2	1.9	0.078
5	0.00	0.12	0.00	74.02	0.00	24.5	1.4	0.076
6	0.00	0.14	0.00	50.40	0.00	45.8	3.7	0.081
7	0.00	0.12	0.00	86.64	0.00	12.5	0.7	0.075
8	0.00	0.11	0.00	82.94	0.00	15.5	1.4	0.078
9	0.00	0.14	0.00	95.81	0.00	3.6	0.5	0.069
10	0.00	0.10	0.00	87.84	0.00	11.1	1.0	0.090

From Table 1 and Fig. 11, it can be concluded that: (i) the largest normalized error between reconstructed displacement fields and displacement fields from FEA evaluated using Eq. (26) is 0.090%; (ii) FEA buckling modes 1~10 are distortional buckling modes dominated by GBT mode 5; (iii) GBT mode 5 (distortional) and mode 7 (local) are the two most significant modes for FEA buckling modes 1~5; (iv) the varying trends of GBT mode amplitudes along the member agree with visual inspection. Taking FEA mode 3 from Fig. 11 for example, the flanges of the Cee are 'closing - opening - closing' from the left end to the right, which is reflected by the amplitude of mode 5 - 'negative - positive - negative'.

Another ability of the modal identification scheme is to decompose the in-plane deformation into combinations of pure modes. The mid-length cross section for buckling mode 1 in Fig. 11 are shown in Fig. 12 demonstrating that the reconstructed displacement fields can be decomposed into contributions of pure modes.

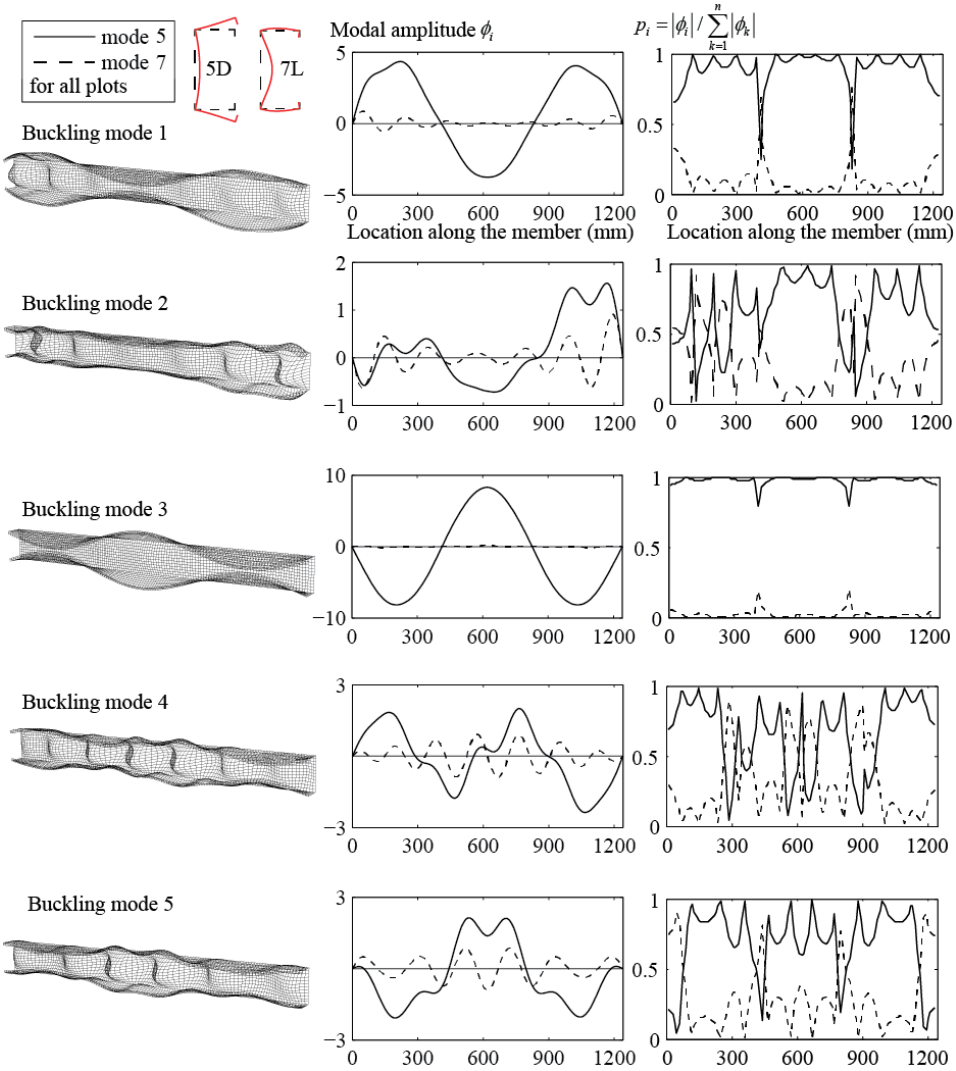

Figure 11: Example 1 - Buckling shapes and modal amplitudes of first 5 buckling modes (modal amplitude has no unit and the unit of length is associated with GBT mode shapes)

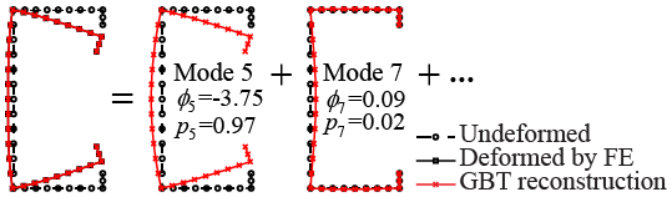

Figure 12: Disp. field reconstruction and decomposing into GBT modes contributions for mid cross section in buckling mode 1

Fig. 13 shows the cross section in Fig. 12 redepicted with annotation of local displacement *v*. It is seen that *v* are close but not strictly the same in each fold line, which 'shifts' the displacement fields slightly out of the sub-domain of GBT solutions. It can be observed the *v* displacement by GBT reconstruction is constant in each fold line as discussed above.

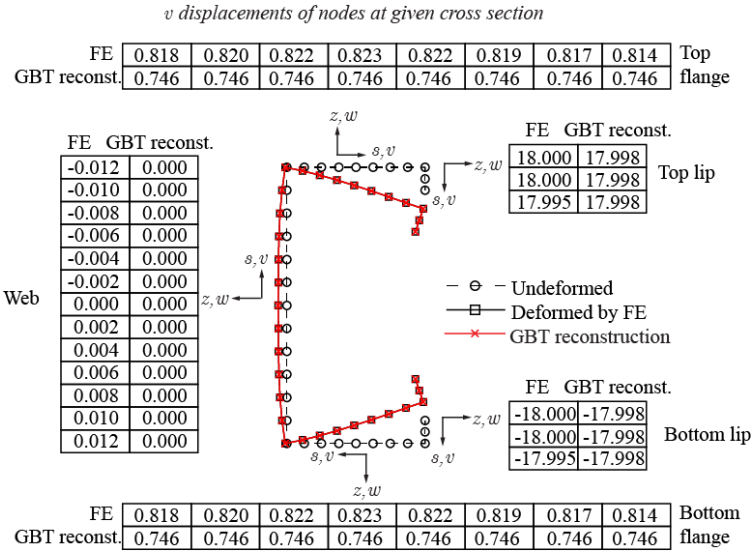

Figure 13: Displacement *v* for mid cross section in buckling mode 1

Example 2 – thin-walled lipped Cee-section beam-column

The second example is conducted on the same structural member and FEA mesh in example 1 but now serving as a beam-column. The left end of the member is fixed against warping for this second analysis. A shell edge traction of q = 16.6667N/mm is applied to the top flange of the right end. Loading and boundary conditions are shown in Fig. 14.

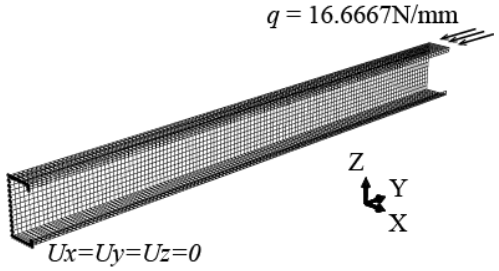

Figure 14: Example 2 - FEA modal boundary conditions

Modal participation and error are evaluated by 'Buckling Cracker' and shown in Table 2. Also, buckling mode shapes and corresponding modal amplitudes of the first 5 buckling modes are shown in Fig. 15.

Table 2: Example 2 - Modal participation and error for the first 10 buckling modes

Buckling mode	2G	3G	4G	5D	6D	7-35L	error (%)
1	4.34	21.25	0.72	50.21	22.50	0.97	0.018
2	0.62	20.73	0.40	47.41	29.78	1.05	0.024
3	0.26	2.49	0.01	58.55	37.84	0.84	0.061
4	0.21	2.12	0.02	59.49	37.26	0.90	0.061
5	0.29	3.14	0.03	61.50	34.12	0.92	0.055
6	0.32	3.08	0.03	60.60	34.72	1.24	0.064
7	0.70	4.44	0.01	56.77	36.10	1.98	0.077
8	1.69	8.27	0.02	56.63	31.18	2.22	0.051
9	2.56	10.71	0.05	58.83	26.66	1.19	0.034
10	2.98	11.21	0.07	55.75	27.39	2.60	0.038

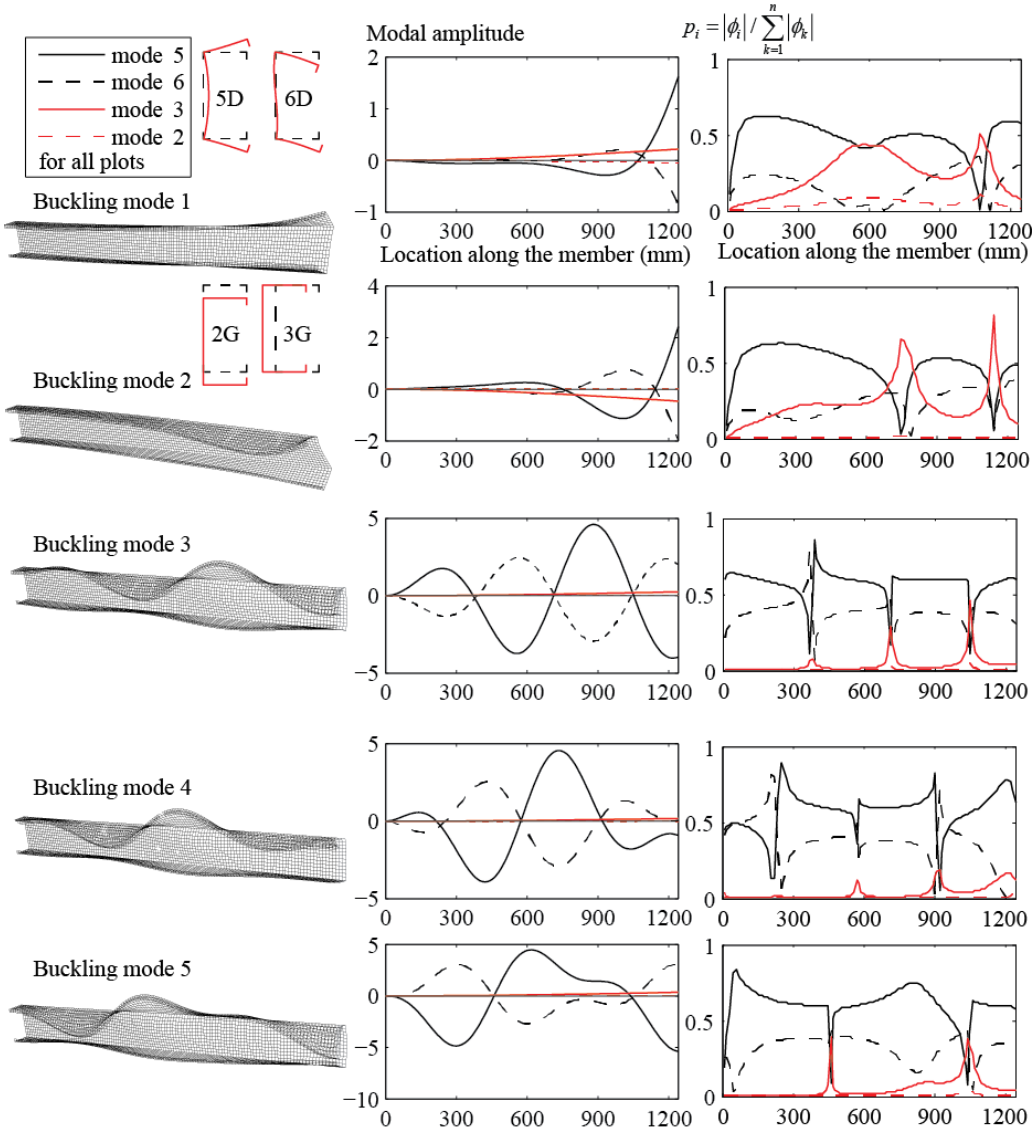

Figure 15: Example 2 - Buckling shapes and modal amplitudes of first 5 buckling modes (modal amplitude has no unit and the unit of length is associated with GBT mode shapes)

From Table 2 and Fig. 15, it can be concluded that: (i) the largest error between reconstructed displacement fields and displacement fields from FEA evaluated using Eq. (26) is 0.077%; (ii) FEA buckling modes 1~10 are distortional buckling modes with domination by GBT mode 5 (distortional); (iii) GBT mode 5 and mode 6 (distortional) are the two most significant modes for FEA buckling modes 1~5; (iv) varying trends of GBT mode amplitudes along the member agree with visual inspection.

5 Conclusions

In this paper, a generalized beam theory (GBT) based modal identification method is presented. Using the method, participation of global, distortional, and local buckling modes can be quantitatively identified from a general 3d displacement field obtained from finite element analysis, experiment, or other computational tools. This method uses GBT cross-sectional mode shapes as basis functions and solves a least squares problem on in-plane displacement fields for determining modal amplitudes.

The proposed approach combines the ideas of displacement-field projection from the constrained finite strip (cFSM) method and GBT stiffness matrix method and utilizes GBT mode shapes . It has several advantages for modal identification: (i) no limitation on member length, and a single set of basis functions can be used for any boundary conditions; (ii) once GBT mode shapes (which are essentially groups of coordinates) are obtained from free tools like GBTUL (Bebiano R. et al. 2014) or Buckling Cracker (Cai 2014), the scheme can be carried out without complex integrals evaluating GBT stiffness terms.

Illustrative examples are provided for both thin-shell finite element eigen-buckling analysis modes demonstrating decomposition of in-plane displacements into a combination of pure modes, The authors are currently making an effort to extend the methodology to members with holes.

Acknowledgements

The authors are greatful for the thoughtful input and guidance provided by Professor Mihai Nedelcu (Technical University of Cluj-Napoca), Professor Dinar Camotim (Technical University of Lisbon), and Dr. Rui Bebiano (Technical University of Lisbon). We are also thankful to Dr. Raymond Plaut, Emertius Professor of Civil and Environmental Engineering at Virginia Tech, for his review and comments.

References

Ádány, S., Joó, A. L., and Schafer, B. W. (2010). “Buckling mode identification of thin-walled members by using cFSM base functions.” *Thin-Walled Structures*, 48(10-11), 806–817.

AISI-S100, N. A. (2007). *North American Specification for the Design of Cold-formed Steel Structural Members. American Iron and Steel Institute, Washington, DC*. AISI, Washition, DC.

Bebiano R., Pina P., Silvestre N., and Camotim D. (2014). *GBTUL*. DECivil/IST, Technical University of Lisbon.

Cai, J. (2014). “Buckling Cracker. ”http://www.moen.cee.vt.edu/category/tools/ and https://www.youtube.com/watch?v=kRsrmb1bWeI accessed Jan. 12, 2015.

Camotim, D., Basaglia, C., and Silvestre, N. (2010). “GBT buckling analysis of thin-walled steel frames: A state-of-the-art report.” *Thin-Walled Structures*, 48(10-11), 726–743.

Davies, J. M., Leach, P., and Heinz, D. (1994). “Second-order generalised beam theory.” *Journal of Constructional Steel Research*, 31(2), 221–241.

Dinis, P. B., and Camotim, D. (2011). “Local/distortional/global mode interaction in simply supported cold-formed steel lipped channel columns.” *International Journal of Structural Stability and Dynamics*, 11(05), 877–902.

Gonçalves, R., Ritto-Corrêa, M., and Camotim, D. (2010). “A new approach to the calculation of cross-section deformation modes in the framework of generalized beam theory.” *Computational Mechanics*, 46(5), 759–781.
Hancock, G. J. (2007). *Design of Cold-formed Steel Structures: To Australian/New Zealand Standard AS/NZS 4600: 2005*. Australian Steel Institute, North Sydney.
Li, Z., Ádány, S., and Schafer, B. W. (2013). “Modal identification for shell finite element models of thin-walled members in nonlinear collapse analysis.” *Thin-Walled Structures*, 67, 15–24.
MALAB. (2010). *MATLAB*. The MathWorks Inc., Natick, Massachusetts.
Nedelcu, M. (2012). “GBT-based buckling mode decomposition from finite element analysis of thin-walled members.” *Thin-Walled Structures*, 54, 156–163.
Nedelcu, M. (2014). “Buckling mode identification of perforated thin-walled members by using GBT and shell FEA.” *Thin-Walled Structures*, 82, 67–81.
Nedelcu, M., and Cucu, H. L. (2014). “Buckling modes identification from FEA of thin-walled members using only GBT cross-sectional deformation modes.” *Thin-Walled Structures*, COUPLED INSTABILITIES IN METAL STRUCTURES, 81, 150–158.
Salomon, A., Tao, F., Cai, J., Moen, C.D. (2015). “Buckling mode identification for a cold-formed steel column experiment with 3D image-based reconstruction.” *Proceedings of the Structural Stability Research Council Annual Conference*, Nashville, TN.
Schardt, R. (1989). *Verallgemeinerte technische biegetheorie*. Springer, Berlin.
Silvestre, N., and Camotim, D. (2002). “Second-order generalised beam theory for arbitrary orthotropic materials.” *Thin-Walled Structures*, 40(9), 791–820.
Silvestre, N., Camotim, D., and Silva, N. F. (2011). “Generalized beam theory revisited: From the kinematical assumptions to the deformation mode determination.” *International Journal of Structural Stability and Dynamics*, 11(05), 969–997.
Simulia. (2012). *Abaqus/CAE*. Dassault Systemes Simulia Corp., RI, USA.